Hydrophilic Monodisperse Magnetic Nanoparticles Protected by an Amphiphilic Alternating Copolymer

Eleonora V. Shtykova,[†] Xinlei Huang,[‡] Xinfeng Gao,[‡] Jason C. Dyke,[‡] Abrin L. Schmucker,[‡] Bogdan Dragnea,[‡] Nicholas Remmes,[§] David V. Baxter,[§] Barry Stein,[||] Peter V. Konarev,[†,⊥] Dmitri I. Svergun,*[,†,⊥] and Lyudmila M. Bronstein*[,‡]

Institute of Crystallography, Russian Academy of Sciences, Leninsky pr. 59, 117333 Moscow, Russia, Department of Chemistry, Indiana University, 800 East Kirkwood Avenue, Bloomington, Indiana 47405, Department of Physics, Indiana University, 727 East Third Street, Bloomington, Indiana 47405, Department of Biology, Indiana University, 1001 East Third Street, Bloomington, Indiana 47405, EMBL, Hamburg Outstation, Notkestraβe 85, D-22603 Hamburg, Germany

Received: June 18, 2008; Revised Manuscript Received: August 8, 2008

Iron oxide nanoparticles (NPs) with diameters of 16.1, 20.5, and 20.8 nm prepared from iron oleate precursors were coated with poly(maleic acid-*alt*-1-octadecene) (PMAcOD). The coating procedure exploited hydrophobic interactions of octadecene and oleic acid tails while hydrolysis of maleic anhydride moieties allowed the NP hydrophilicity. The PMAcOD nanostructure in water and the PMAcOD-coated NPs were studied using transmission electron microscopy, ζ-potential measurements, small-angle X-ray scattering, and fluorescence measurements. The combination of several techniques suggests that independently of the iron oxide core and oleic acid shell structures, PMAcOD encapsulates NPs, forming stable hydrophilic shells which withstand absorption of hydrophobic molecules, such as pyrene, without shell disintegration. Moreover, the PMAcOD molecules are predominantly attached to a single NP instead of self-assembling into the PMAcOD disklike nanostructures or attachment to several NPs. This leads to highly monodisperse aqueous samples with only a small fraction of NPs forming large aggregates due to cross-linking by the copolymer macromolecules.

Introduction

Magnetic nanoparticles (NPs) have received considerable attention because they hold promise of many exciting applications, such as magnetic storage media,[1−3] ferrofluids,[4−6] biosensors,[7] contrast enhancement agents for magnetic resonance imaging,[8−11] bioprobes,[12,13] catalysis,[3] etc. Because magnetic properties are size-dependent,[3,14−16] obtaining narrow NP size distribution is an important requirement in magnetic NP syntheses. Monodisperse iron oxide NPs can be prepared by thermal decomposition of iron acetylacetonates[1,17,18] or carboxylates[18−20] in high-boiling solvents containing surfactants (oleic acid, oleylamine, etc.). As recently reported,[21] the mechanism of thermal decomposition of a precursor (a "heating-up" process) is similar to that of a "hot injection" method in separation of nucleation and growth events, leading to monodisperse NPs.

Typically, NPs prepared via thermal decomposition of a precursor are hydrophobic, whereas for many applications, including biomedical functions, the NPs should be hydrophilic. Several methods were suggested to hydrophilize hydrophobic nanoparticles: ligand exchange,[22−26] attachment of polymer chains on nanoparticle surface,[27,28] formation of NPs in the presence of polymeric surfactants,[29] or encapsulation of the NPs with amphiphilic molecules thanks to formation of hydrophobic double layers.[30−32] We believe that the last method is especially robust and facile for NP hydrophilization.[30−32] The encapsulation of monodisperse iron oxide NPs by PEGylated phospholipids was described earlier.[33,34] This method yielded exceptionally stable and biocompatible NPs, but the high price of PEGylated phospholipids limits their potential applications for NP hydrophilization and stimulates the search for more affordable amphiphilic molecules.

Alternating amphiphilic copolymers proved to be good candidates for NP functionalization.[35,36] The hydrophilization of hydrophobic nanoparticles using short (7300 Da) poly(maleic anhydride-*alt*-1-tetradecene) was described by Pellegrino et al.[35] To stabilize the polymer coating, the authors used bis(6-aminohexyl)amine cross-linking the shell via interaction with anhydride moieties. Solubility in water was achieved by hydrolysis of the remaining anhydride moieties. The largest NPs stabilized by this method did not exceed 9.2 nm, and no structural studies were performed on these NPs. In the present paper, we report on a simplified procedure of stabilization of large magnetic NPs (16−21 nm in diameter) with a much longer alternating block copolymer (30 000−50 000 Da), poly(maleic anhydride-*alt*-1-octadecene) (PMAOD). Interestingly, hydrolysis of PMAOD in water leads to poly(maleic acid-*alt*-1-octadecene), PMAcOD, where maleic acid units are highly hydrophilic. We believe that the longer copolymer chains used here provide a stable NP shell without additional cross-linking and loss of carboxy functionality, whereas the longer hydrophobic tail (C_{16} vs C_{12} in the previously studied copolymer[35]) allows a more stable hydrophobic double layer. In a recent paper by Di Corato et al.,[37] the same PMAOD was used, as well, for NP hydrophilization; however, the authors again employ cross-linking with an amine for coating stabilization, which we prove unnecessary. PMAOD was also recently used for coating of

* To whom correspondence should be addressed. E-mail: (L.M.B.) lybronst@indiana.edu, (D.I.S.) svergun@embl-hamburg.de.
† Russian Academy of Sciences.
‡ Department of Chemistry, Indiana University.
§ Department of Physics, Indiana University.
|| Department of Biology, Indiana University.
⊥ EMBL.

10.1021/jp8053636 CCC: $40.75
Published on Web 10/01/2008

magnetic NPs after alteration with poly(ethylene glycol) (PEG) chains;[36] however, it seems to be reasonable only for certain applications.

In the present work, both PMAcOD self-assembling in water and structure of NPs coated with PMAcOD were comprehensively characterized for the first time using small-angle X-ray scattering (SAXS), transmission electron microscopy (TEM), ζ-potential measurements, and fluorescence studies of the pyrene uptake. X-ray powder diffraction (XRD) and FTIR were used for the NP characterization.

Among methods providing structural information about complex polymer or composite polymer/NP structures, SAXS holds special advantages due to its capability to comprehensively characterize sophisticated polymer matrices, the NP size distributions in them, and the structural changes occurring during the NP formation processes. Importantly, specimens are studied in their natural media and aggregate states.[38] In our preceding work, we have studied structural characteristics of different kinds of novel advanced nanomaterials at resolution from about 1 to 100 nm.[39−44] SAXS allowed us to obtain size distributions of metal NPs, their locations in metal containing polymer matrices,[39−42,45,46] and structural information about internal organization of the entire system.[41−44] Novel methods for SAXS data analysis originally developed for biological systems[47−49] were for the first time successfully applied to complex polymers systems, including those containing metal nanoparticles.[34,41,50,51] In the present paper, SAXS allows us to address the major concern of using high molecular weight alternating copolymer: NP aggregation due to attachment of one copolymer molecule to several NPs. SAXS reveals highly homogeneous populations of individual NPs showing only a marginal fraction of cross-linked aggregates and demonstrating that in the vast majority of cases, a copolymer molecule interacts with a single NP.

Experimental

1. Materials. $FeCl_3 \cdot 6H_2O$ (98%), and docosane (99%) were purchased from Sigma-Aldrich and used as received. Hexanes (85%), ethanol (95%), and acetone (99.78%) were purchased from EMD and used as received. Chloroform (Mallinckrodt, 100%), oleic acid (TCI, 95%), TBE buffer (1.3 M Tris, 450 mM boric acid, 25 mM EDTA·Na_2 in H_2O, Fluka), and oleic acid sodium salt (ScienceLab.com, 95%) were used without purification. PMAOD (30 000−50 000 Da, Aldrich) was used as received. Water was purified with a Milli-Q (Millipore) water purification system (18 μS). Pyrene (98%, Aldrich) was recrystallized twice from ethanol and sublimed in vacuum at 80 °C.

2. Synthetic Procedures. ***2.1. Synthesis of Iron Oxide Nanoparticles.*** The synthesis of iron oleate was carried out using a published procedure.[20] The resultant iron oleate was either dried at 70 °C in a vacuum oven for 24 h (notation FeOl2, see ref.[52]) or first extracted with ethanol and acetone to remove impurities, including oleic acid, and then dried at the above conditions (notation FeOl4; see ref 52). The spherical iron oxide nanoparticles with mean diameters of 16.1 nm (3.7% standard deviation, **NP1**) and 20.5 nm (4.1% standard deviation, **NP2**) were synthesized using thermal decomposition of FeOl4.[53] In a typical experiment for **NP1**, 1.39 g (1.5 mmol for the molecule containing three oleates per one Fe) of FeOl4, 1.6 mL of oleic acid (5 mmol), and 7.7 g of docosane (hydrocarbon $C_{22}H_{46}$, solid at room temperature) were mixed in a three-neck, round-bottom reaction flask, and the flask was degassed four times using "evacuation-filling with argon" cycles, ending with filling with argon. Then the mixture was first heated to 60 °C to melt the solvent and allow the reactants to dissolve under vigorous stirring. Then the temperature was increased to 370 °C with a heating rate of 3.3 °C/min (using a digital temperature controller with an attached Glas-Col heating mantel and set temperature of 380 °C) under vigorous stirring and refluxing for 3 min. The resultant solution was then cooled down to 50 °C, and a 50 mL mixture of hexane and acetone (volume ratio 1:1) was added into the reaction flask to precipitate the NPs. The NPs were separated by centrifugation and washed three times by a mixture of hexane and acetone (volume ratio 1:3). After washing, the resultant NPs were again centrifuged and dissolved in chloroform for long-term storage. (Alternatively, the solid reaction solution can be stored in a refrigerator, and aggregation-free NPs can be collected and washed directly when needed.) **NP2** was prepared in a similar fashion using 1.5 mL of oleic acid. The 20.8 nm NPs (4.0% standard deviation **NP3**) were prepared according to the procedure described in our preceding papers using FeOl2 as a precursor.[34,52]

2.3. Encapsulation of Iron Oxide Nanoparticles with PMAcOD. To encapsulate the iron oxide nanoparticles in PMAOD, a stock solution of PMAOD in $CHCl_3$ was made with a concentration 0.01 g/mL. The solution of 1 mg of iron oxide NPs in 1 mL of chloroform was added to 1 mL of the PMAOD solution and allowed to stir for 1 h. Chloroform was then removed under vacuum, and 2 mL of 20% TBE buffer was added. Then the solution was sonicated for 10 min and heated at 60 °C for an additional 10 min. Aggregates were removed by centrifugation at 3000 rpm (twice for 15 min), and excess polymer and TBE buffer were removed by ultracentrifugation (1 h, 90 000 rpm, 4 °C), followed by filtration centrifugation using 0.4 μm Millipore filters (10 min, 6000 rpm, 3 times). The final product was then analyzed to confirm uniformity and absence of free polymer using TEM and DLS. The yield of the purified particles was 90%.

2.4. Hydrolysis of PMAOD Polymer. PMAOD solution (0.8 mL, 0.01 g/mL in $CHCl_3$) was evaporated in a vacuum oven. To the dried sample, 3 mL of 20% TBE buffer was added, and the solution was stirred for 72 h. The solution was then heated to 60 °C for 1 h and stirred at room temperature for an additional 24 h. The product was purified by dialysis against deionized water for 24 h.

2.5. Preparation of Samples for Fluorescence Spectroscopic Analysis. To prepare the 6×10^{-7} M pyrene aqueous solution (the concentration of a saturated pyrene solution in water is 7×10^{-7} M), 10 μL of the pyrene ethanol solution (1 mg/mL) was evaporated in a flask under a flow of nitrogen, and then the flask was charged with 82 mL of Milli-Q water. The resultant solution was stirred overnight in the dark.

To prepare a solution containing 6×10^{-7} M pyrene and iron oxide NPs coated with PMAcOD, 10 μL of the pyrene ethanol solution with a concentration of 0.1 mg/mL was evaporated in a flask, and then 1.65 mL of the 0.7 mg/mL **NP3**−PMAcOD aqueous solution was added, and the mixture was stirred for 24 h in the dark. In addition, the above solution was diluted with a 6×10^{-7} M pyrene aqueous solution to obtain the final solutions with concentrations of 0.35, 0.07, and 0.007 mg/mL. Each solution was stirred for 24 h in the dark for equilibration.

3. Characterization. FTIR spectra were recorded on a Nicolet spectrometer by placing the sample on a KBr disk and evaporating the chloroform or THF.

ζ-Potential measurements were performed using a Malvern Zetasizer Nano ZS equipped with an MPT-2 autotitrator

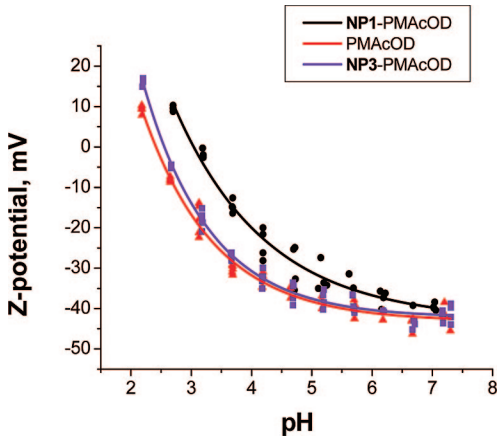

Figure 1. ζ-Potential as a function of pH for PMAcOD and **NP1** and **NP3** coated with PMAcOD.

containing HCl (0.1 M and 0.01 M) and NaOH (0.1 M). The software was programmed to titrate the solutions from pH 7.5 down to pH 2.5−3 in increments of 0.5 pH. ζ-Potential and pH values were measured before and after sample recirculation through the folded capillary cell. Data was processed using the absorption of bulk iron oxide, the indices of refraction of iron oxide and solvent, and the viscosity of the pure water. The Smoluchowski approximation was used to convert the electrophoretic mobility to a ζ-potential.

Electron-transparent specimens for TEM were prepared by placing a drop of a dilute solution onto a carbon-coated Cu grid. Images were acquired at an accelerating voltage of 80 kV on a JEOL JEM1010 transmission electron microscope. Images were analyzed with the Adobe Photoshop software package and the Scion Image Processing Toolkit to estimate NP diameters. Normally, 150−300 NPs were used for analysis.

X-ray diffraction patterns were collected on a Scintag theta-theta powder diffractometer with a Cu Kα source (0.154 nm).

The synchrotron radiation X-ray scattering experiments were performed on the X33 camera[54] of the European Molecular Biology Laboratory (EMBL) on the storage ring DORIS III of the Deutsches Elektronen Synchrotron (DESY, Hamburg). A MAR Image plate detector was used to collect the scattering data in the range of the momentum transfer $0.1 < s < 5.0\ \text{nm}^{-1}$, where $s = (4\pi \sin\theta)/\lambda$, 2θ is the scattering angle, and $\lambda = 0.15$ nm is the X-ray wavelength. PMAcOD and iron oxide nanoparticles coated with PMAcOD (**NP1**-PMAcOD) in solution were measured with exposure times of 2 min in a vacuum cuvette to diminish the parasitic scattering. Concentrations of the samples in the range 0.1−1.0 mg/mL were chosen to minimize interaction of the particles. Primary data processing was carried out using standard procedures.[55] To determine distance distribution functions $p(r)$ of the samples, an indirect transform program GNOM[56] was used. An ab initio method of structural modeling (program DAMMIN [46]) was employed to reconstruct the low-resolution shape and internal structure of the iron oxide cores of the NPs.

The spatial structure of the −MAcOD− units of the alternating copolymer was modeled by Cerius2 (version 3.5, MSI/Accelrys).[57] The first step was to construct a single −MAc−OD− unit. Because of chirality of the two linkage carbons of the −MAc− subunit and one linkage carbon of the −OD− subunit, the −MAcOD− unit can adopt up to eight possible configurations. Correspondingly, eight models were created for the −MAcOD− unit. They were designed as RRR, RRS, RSR, RSS, SRR, SRS, SSR, and SSS, respectively where R (rectus) and S (sinister) indicate the configuration of the corresponding chiral carbon. In the second step, each model of the −MAcOD− unit was solely used to build a short PMAcOD polymer chain consisting of 10 −MAcOD− units with an extended conformation, generating eight models of the PMAcOD polymer chain correspondingly. Energy minimization was carried out for each PMAcOD polymer model. The resulting structures of the short PMAcOD polymer chain were consequently used to construct models of self-association of this polymer in solution. These structures were taken into use in two ways: (i) a structure was entirely taken as a building block or (ii) a structure fragment of one −MAcOD− unit was taken from the structure and used as a basic building unit. Bilayer assemblies of different geometrical shapes were constructed, and their SAXS patterns were calculated using the program CRYSOL[48] and compared with the experimental scattering to find the overall organization of the alternating copolymer in solution best fitting the SAXS data. The agreement between the experimental data $I_{\text{exp}}(s)$ and those calculated from the models was characterized by the discrepancy

$$\chi^2 = \frac{1}{N-1}\sum_j \left[\frac{I_{\text{exp}}(s_j) - cI_{\text{calc}}(s_j)}{\sigma(s_j)}\right]^2 \quad (1)$$

where N is the number of experimental points, c is a scaling factor and $I_{\text{calc}}(s_j)$ and $\sigma(s_j)$ are the calculated intensity and the experimental error at the momentum transfer s_j, respectively.

Magnetic measurements were carried out using a Quantum Design MPMS XL magnetometer. Zero-field cooling curves were taken by cooling the sample in null field (±0.1 Oe) down to 4.5 K, applying a 50 Oe field, and then measuring the magnetization in regular temperature increments up to 300 K. For the FC curves, the samples were cooled in the 50 Oe field to 4.5 K and magnetization measurements were repeated in regular temperature increments up to 300 K.

Fluorescence spectra were recorded on a Perkin-Elmer LS-50B luminescence spectrometer equipped with a thermo NESLAB RTE-140 low-temperature bath circulator for temperature control. All measurements were carried out at 25 °C unless stated otherwise. For measurements of the emission spectra, the excitation and emission slits were set at 5 and 3.5 nm, respectively. The excitation wavelength was set at 330 nm, and spectra were recorded from 350 to 550 nm with a scan rate of 200 nm/min.

Results and Discussion

1. Synthesis and Characterization Using ζ-Potential Measurements. In this work, we used three NP samples for the PMAcOD coating: **NP1** (16.1 nm), **NP2** (20.5 nm), and **NP3** (20.8 nm). **NP1** and **NP2** were prepared from the same iron oleate with a notation FeOl4. FeOl4 was subjected to additional purification to remove oleic acid uncontrollably formed during the iron oleate synthesis and included in the iron oleate structure.[52] This precursor required the addition of the increased amount of oleic acid (capping molecules) during the NP synthesis for the successful NP stabilization (see Experimental Section and the Supporting Information, SI). **NP3** was prepared from the other iron oleate precursor with a notation FeOl2, which was thermally treated after synthesis, but no oleic oleate was removed.[52] The TEM images and XRD spectra of the NPs synthesized are presented in (SI, Figures S1 and S2). The latter demonstrate that the crystalline structure is similar in all the samples. The magnetic measurements indicate that NPs are superparamagnetic (see SI, Figure.S3).

According to the FTIR data of the **NP1** and **NP3** samples (see SI, Figure S4 for details), the former NPs contain a larger

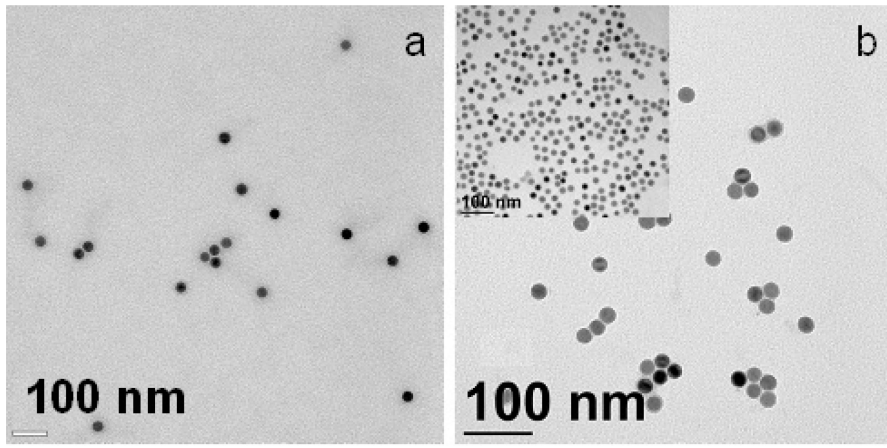

Figure 2. TEM images of **NP1**−PMAcOD (a) and **NP3**−PMAcOD (b) cast from aqueous solutions. Inset in b shows lower magnification image.

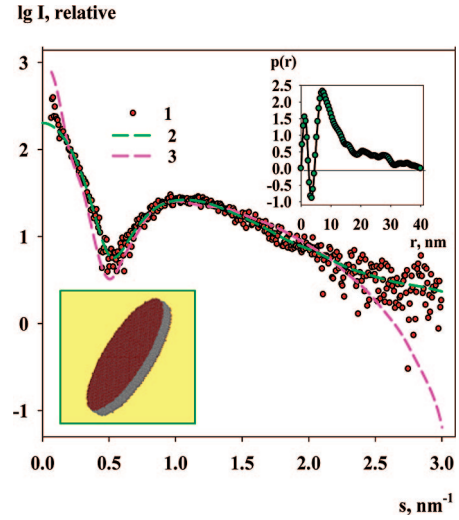

Figure 3. The experimental SAXS data from PMAcOD copolymer in solution (1) and the distance distribution function $p(r)$ computed by GNOM (inset). The smooth curve (2) is backtransformed from $p(r)$ and extrapolated to zero scattering angle. The smooth curve (3) is a typical best fit from a disklike bilayer constructed from atomic models of individual −MAcOD− units.

fraction of oleic acid than the latter NPs, yet in the former case, poorly adsorbed oleic acid is present (see SI, Scheme S1). Thus, **NP1** and **NP2** have similar oleic acid shell but different sizes, whereas **NP2** and **NP3** have similar sizes but different shell structures.

We expected that the presence of the extra amount of oleic acid in **NP1** and **NP2** might impede the encapsulation by PMAOD due to disruptions in the formation of a hydrophobic double layer. The encapsulation with PMAOD was carried out by first dissolving PMAOD in the chloroform solution of NPs, followed by evaporation of the chloroform and addition of 20% of TBE buffer with subsequent sonication, heating, and purification. It is noteworthy that the excess of PMAcOD (formed upon hydrolysis of PMAOD) should be removed promptly from the NP sample to prevent etching of iron oxide NPs.

To our surprise, independently of the NP type and size, stable NPs coated with PMAcOD were formed. We assume that in the presence of PMAOD, the replacement of the extra oleic acid molecules nonadsorbed on the NP surface is favored due to cooperative interactions of the PMAcOD units and the entropy increase. The NPs coated with PMAcOD are stable for months and do not require any additional stabilization, such as shell cross-linking with amines.[35]

For comparative structural studies of NPs and a copolymer, we carried out hydrolysis of PMAOD in 20% TBE buffer to prepare PMAcOD. Because PMAcOD is an amphiphilic alternating copolymer, we expected that it would self-assemble in water, forming some finite ordered structures (see below) where hydrophobic moieties are located in the interior of these structures for energy minimization, whereas carboxy groups (or carboxylates) are exposed to water. As was suggested in ref 58, self-assembling of the other amphiphilic alternating copolymer, poly(maleic acid-*alt*-styrene) (PMAcSt), leads to formation of stacked nanotubes.

To estimate the charges of both PMAcOD and NPs coated with this polymer, ζ-potential measurements were taken for PMAcOD, **NP1**−PMAcOD, and **NP3**−PMAcOD. As can be seen from Figure 1, the ζ-potentials of PMAcOD and **NP3**−PMAcOD are nearly the same in a wide pH range, whereas for **NP**1, the ξ-potential values are lower. Remember that in the **NP1** sample, the NPs are smaller (16.1 nm) than in **NP3** (20.8 nm). We observed a similar trend for 20.1 and 8.5 nm NPs coated with carboxy-terminated PEGylated phospholipids (see ref 33), and we believe this is caused by a different NP curvature, leading to a different charge density in the NP exterior (lower for the smaller NPs and higher for the larger NPs). The similarity of the ζ-potentials of PMAcOD and **NP1**−PMAcOD suggests the similar charge density on the nanostructure surface. At pH 7, the ξ-potential of **NP3**−PMAcOD is about −40 mV, which is comparable to that of PEGylated phospholipid-coated NPs used as successful templates for Brome Mosaic Virus capsid self-assembling.[33]

Figure 2 shows TEM images of **NP1** and **NP3** coated with PMAcOD. This figure demonstrates that the NPs stay intact (no etching) and do not aggregate.

3. Characterization by SAXS. SAXS measurements were employed to characterize the structural organization of PMAcOD and the **NP1**−PMAcOD sample in aqueous solutions. To the best of our knowledge, the self-assembling of PMAcOD in water was never studied before, while SAXS studies of self-organization of other alternating amphiphilic copolymers are scarce.[58]

3.1. PMAcOD Self-assembling: SAXS and Modeling. The experimental scattering profile from the PMAcOD copolymer in solution is shown in Figure 3. The distance distribution function $p(r)$ calculated from the experimental data (Figure 3, inset) reveals the maximum size of the particles of about 40 nm and displays negative values in the range of interatomic distances around 3−4 nm. These negative values are typical

SCHEME 1: Modeling and Search for the Best Fits[a]

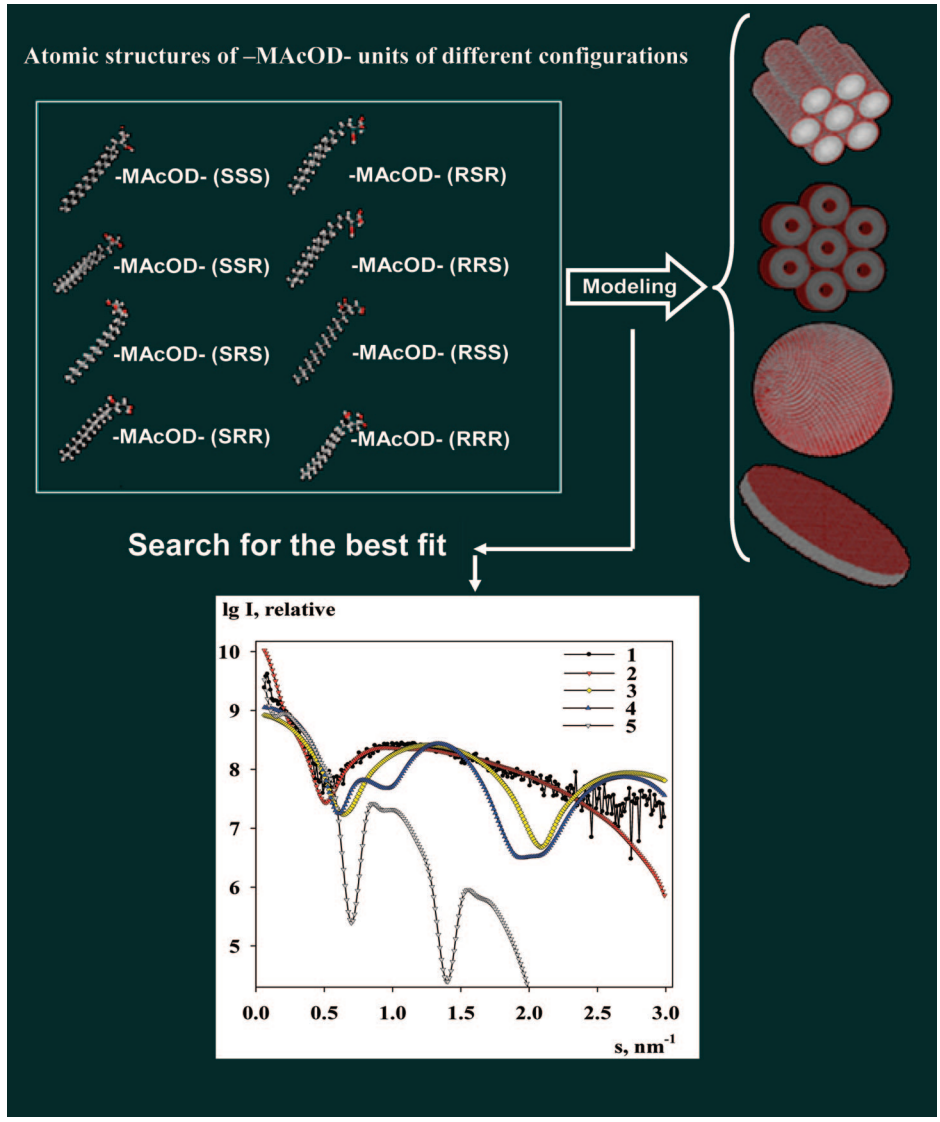

[a] In the figure inside the scheme: experimental scattering curve from the PMAcOD copolymer in solution (1) and the best fits to the experimental profile of the scattering patterns computed from disks (2), solid (3), and hollow (4) cylinder-shape aggregates, and bicelles (5), constructed using atomic structures of the −MAcOD− units.

for lipid bilayer structures and appear due to the hydrophobic regions in the copolymer, which have a lower electron density than water. The distances of 3−4 nm correspond to the double layer formed by the hydrophobic tails of the PMAcOD unit (1.6 nm for a single tail).

To assess the organization of the PMAcODs' self-assemblies in solution, models were constructed from the energy-minimized single −MAcOD− units and short PMAcOD chains as described in the Experimental Section. Monolayers consisting of the −MAcOD− units in eight different configurations reflecting possible chirality of the linkage carbons were employed to construct micelles and cylinder-shaped aggregates. Further, bilayered structures were employed to produce hollow cylinders, bicelles, and disks (Scheme 1). All of the models were constrained by the experimental maximum size of the aggregate $D_{max} = 40$ nm. The scattering intensities from the models were computed using CRYSOL,48, and the discrepancy χ was calculated between the experimental data and the model scattering. The best fits obtained in each class of shapes are shown in Scheme 1. The disklike bilayers (curve 2) clearly yield the best agreement with the experimental data ($\chi \approx 1.9$), whereas all scattering profiles from the other types of models failed to provide good fits ($\chi > 5$).

The scattering patterns calculated from all eight disklike structures constructed from the different configurations of the −MAcOD− units gave very similar fits. All best disklike models had a diameter of 40 nm and a thickness of the bilayer of 3.2 nm, in agreement with the results of GNOM analysis of the $p(r)$ function.

We also attempted to construct models from the building blocks consisting of 10 −MAcOD− units obtained by molecular modeling (see the Experimental Section and SI). The disklike models with $D = 40$ nm and thickness 3.2 nm again yielded the best fits, albeit showing features at higher angles that were not present in the experimental SAXS data (see example in the SI, Figure S6). Most importantly, the modeling by short chains further confirmed the shape of the self-assembled PMAcOD to be a disklike bilayer. Similar shapes for ensembles of amphiphilic molecules, mostly for phospholipids, are described in the literature.[59−62]

3.2. Nanoparticles Coated with PMAcOD. The experimental scattering profile from **NP1**−PMAcOD in solution shown in

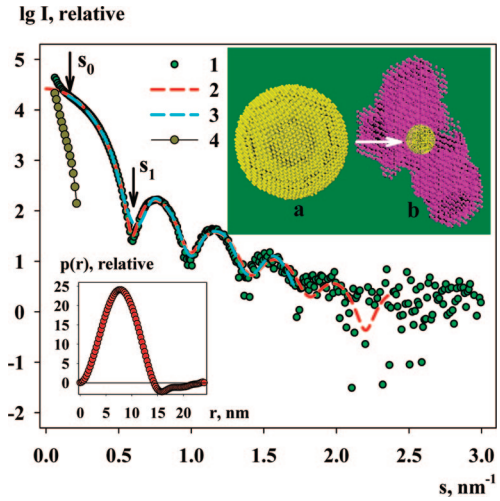

Figure 4. Scattering patterns from the aqueous solution of **NP1**−PMAcOD: experimental data (1); the curve processed by GNOM and extrapolated to zero angle (2); scattering from the ab initio model of the NP1 core (3); the difference scattering from the **NP1**−PMAcOD aggregates (4). Insets: bottom left, distance distribution function; top right, ab initio bead models of the individual NP core (a) and of the cluster (b) reconstructed from the scattering data. Note that part b is not to scale with part a, but the shape of the NP core is superposed on the shape of the aggregate as a scale indicator.

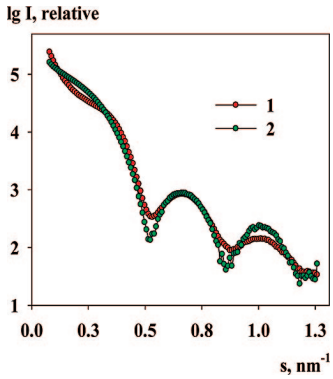

Figure 5. Comparison of the experimental SAXS profiles from PEG-PL-coated NPs with a diameter of 20.1 nm[34] (1) and from the **NP1**−PMAcOD NPs (2). The angular axis for the former sample was multiplied by 0.8 to account for the difference in the sizes of the iron core.

Figure 4 (curve 1) displays distinctive maxima characteristics for practically monodisperse systems of spherical particles.

This scattering is dominated by the contribution from the metal, which has a much higher contrast than the amphiphilic copolymer. The average radius of the iron oxide cores can thus be directly estimated from the position of the first minimum, s_1 (Figure 4) as[38] $R = 4.49/s_1$. This value was found to be 7.9 nm, which correlates well with nanoparticle diameter of 16.0 nm from TEM. The initial portion of the SAXS pattern (scattering vectors less than $s_0 \approx 0.2$ nm^{-1}) displays an upward trend, indicating that a small portion of large aggregates is present in the **NP1**−PMAcOD solution. To extract the contribution due to individual particles, the scattering pattern in the range $s > s_0$ was processed by the indirect transformation program GNOM[56] to compute the distance distribution function $p(r)$ (Figure 4, bottom left inset). In the range of interatomic distances below 15 nm, the bell-shaped $p(r)$ function resembles that of a spherical particle but at larger distances slight negative excursion is observed up to $D_{max} \approx 22.5 - 23.0$ nm. These negative values of $p(r)$ are clearly due to the negative contrast of the hydrophobic

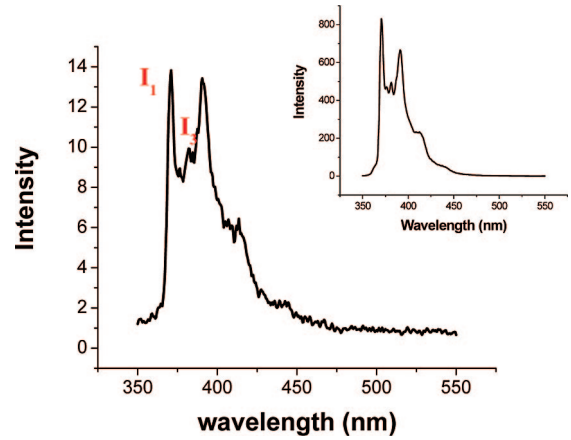

Figure 6. Fluorescence emission spectrum of pyrene in the 0.07 mg/mL **NP3**−PMAcOD aqueous solution. Inset shows the 6×10^{-7} M solution of pyrene in water.

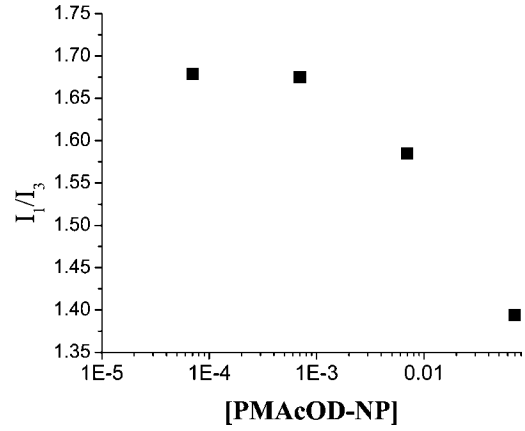

Figure 7. Dependence of I_1/I_3 on the **NP3**−PMAcOD concentration in aqueous solutions.

PMAcOD tails against water, and this allows one to estimate the thickness of the hydrophobic double layer formed by PMAcOD + oleic acid as (22.5 − 16.0)/2 nm or (23.0 − 16.0)/2 nm ≈ 3.2 − 3.5 nm, in agreement with the length of both hydrophobic tails partially interdigitated. No similar structures to those observed for pure PMAcOD in water were detected, suggesting that inclusion of the PMAcOD molecules in the NP shell is more favorable than their free self-assembling in the presence of NPs.

The back-transformed $p(r)$ function yielded the scattering pattern of a single **NP1**−PMAcOD particle (Figure 4, curve 2), which was subtracted from the experimental SAXS data to yield an estimate of the scattering from the aggregates (Figure 4, curve 4). The shapes of the nanoparticles and of the aggregates were reconstructed ab initio from the corresponding scattering patterns by the program DAMMIN.[46] A typical shape of the **NP1**−PMAcOD particle represented by an ensemble of densely packed beads (upper inset in Figure 4) yields a good fit to the experimental data in the range $s > s_0$ with discrepancy $\chi = 1.2$ (curve 3 in Figure 4). Note that the shape reflects solely the structure of the iron oxide core, thanks to its high positive contrast. The multilayered interior of the model reflects the process of the formation of the iron oxide core from smaller nuclei, as discussed in our preceding paper.[34] The shape of the aggregates, also presented in the upper inset of Figure 4, reveals an irregular conglomerate containing about 30−40 individual **NP1**−PMAcOD particles (in panel b, the aggregate is superimposed onto the single particle). Because the zero-angle

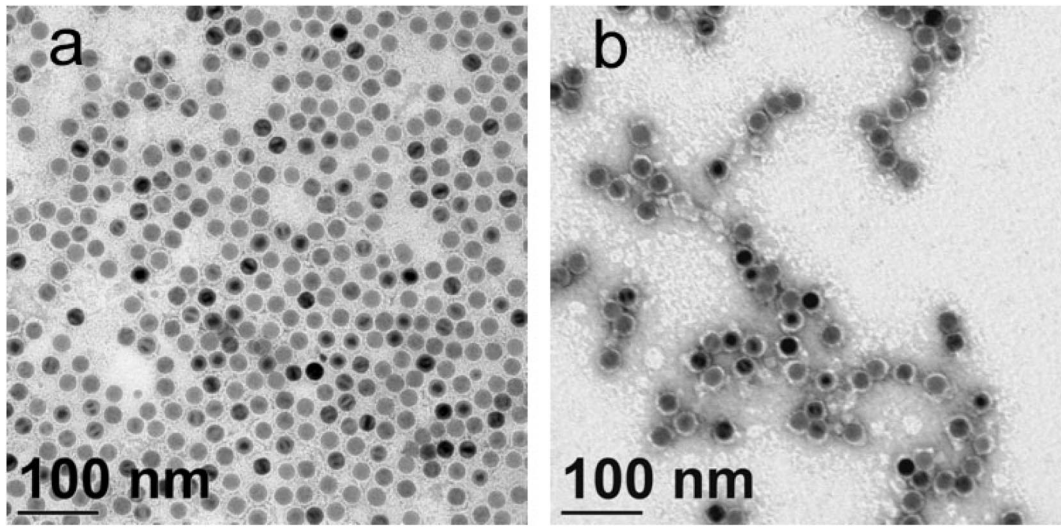

Figure 8. TEM images of **NP3**−PMAcOD before (a) and after (b) pyrene uptake. The TEM grids were stained with uranyl acetate to accentuate the shell.

scattering $I(0)$ is proportional to the squared volume and the volume fraction and the aggregates (curve 4) yield practically the same $I(0)$ value as the **NP1**−PMAcOD particles (curve 2), the volume fraction of the aggregates in the sample does not exceed 0.1%.

It is interesting to compare the present results with those obtained earlier for iron oxide nanoparticles encapsulated by phospholipids with poly(ethylene glycol) tails (PEG-PL).[34] In the latter paper, SAXS revealed dynamic clusters consisting, on average, of four individual particles, and a question may arise whether and how a system containing clusters of a few particles can be distinguished from a largely monodisperse system of individual particles containing a small fraction of large clusters. In Figure 5, the scattering from the PEG-PL-coated nanoparticles taken from ref 34 (curve 1) is superposed with the experimental scattering from **NP1**−PMAcOD solution (curve 2); the angular scale of the former pattern was multiplied by a factor of 0.8 taking into account the difference in size between the two types of nanoparticles). The system of the PEG-PL-coated nanoparticles displays a characteristic scattering profile with a shoulder at small angles reflecting interference among the particles within the clusters, whereas the scattering from **NP1**−PMAcOD does not display any interference effects, but shows a moderate upturn at very small angles (i.e., very large sizes). One can therefore conclude that **NP1**−PMAcOD NPs in solution are not cross-linked by the alternating polymer but, instead, remain largely as individual nanoparticles.

4. Pyrene Uptake: Fluorescence Measurements. Because hydrophilization of hydrophobic NPs is carried out due to hydrophobic interactions, it is important to evaluate the stability of such amphiphilic shells. One might suggest that the presence of hydrophobic or amphiphilic molecules in the NP solutions might destroy the hydrophobic double layer, leading to NP precipitation. To investigate the stability of the hydrophobic double layer, we studied uptake of a hydrophobic molecule, pyrene, using fluorescence measurements.[63,64] It is known that pyrene has a very distinctive fluorescence spectrum whose characteristics change depending on the polarity of the surrounding medium. Typically, the ratio of the intensities of peak 3 (I_3 at 385 nm) to peak 1 (I_1, 0−0 band at 374 nm)[63] or vise versa[64] are used to characterize the pyrene environment. In water, I_1/I_3 is in the range 1.7−1.8, but in hydrophobic solvents or in surfactant micelles, this value is 1.10.[65]

Figure 6 shows fluorescence emission spectra of **NP3**−PMAcOD and of pure pyrene (inset). The I_1/I_3 changes from 1.71 for water to 1.39 for the 0.07 mg/mL **NP3**−PMAcOD solution, revealing that pyrene partitions into the hydrophobic layer.

Figure 7 displays a dependence of I_1/I_3 on the **NP3**−PMAcOD concentration in aqueous solutions. Even at a concentration of 0.007 mg/mL, some pyrene molecules have a hydrophobic microenvironment, whereas at further dilution, the **NP3**−PMAcOD influence on fluorescence is hardly noticeable. It is noteworthy that at **NP3**−PMAcOD concentrations of 0.35 and 0.7 mg/mL, the pyrene fluorescence is completely quenched. This quenching might be ascribed to close packing of pyrene molecules in the hydrophobic double layer of the NP shells, but normally, the quenching with a neighboring pyrene molecule results in excimer formation,[66] the emission of which is not observed in our case. In a control experiment, we demonstrated that the presence of PMAcOD in solution in concentrations equal to or higher than the NP concentration of 0.7 mg/mL does not quench the pyrene emission, but in the solid mixed film consisting of PMAcOD and pyrene, pyrene is partially quenched. We believe that the pyrene quenching in the PMAcOD shell of iron oxide NPs should be due to a change of the pyrene packing conformation (compared to pure pyrene), probably combined with adsorption and subsequent charge-transfer interaction with the nanocrystal, as was discussed by Turro et al. for functionalized pyrenes and γ-Fe_2O_3 NPs.[67]

Figure 8 shows the TEM images of **NP3**−PMAcOD before and after pyrene uptake. The TEM grids were stained with uranyl acetate to accentuate the shells. Because the shell exterior is decorated with carboxyl groups, uranyl cations form clear dark lines around NPs. The shell size calculated based on 200 NPs (in four shell locations of each particle) is 3.3 nm with a standard deviation of 25%. This value is consistent with a double layer of hydrophobic tails (fully extended oleic acid and octadecene tails) with partial interdigitation, matching SAXS data. A close look at Figure 8a suggests that the stain penetrates beyond the NP exterior toward the iron oxide core, revealing that the shell is not dense. After incorporation of pyrene, the shell size slightly increases to 3.7 nm (with a standard deviation of 6.3%), thus matching the size expected for a hydrophobic double layer. The shell also becomes very dense, appearing white on the TEM image (Figure 8b). This is consistent with

densely packed pyrene between hydrophobic tails, leading to the increase in the shell density.

Conclusions

Stable hydrophilic NPs were prepared by encapsulation of hydrophobically coated monodisperse iron oxide NPs of 16−21 nm in diameter and with different surface properties using alternating copolymer PMAOD. After hydrolysis, this copolymer forms disklike structures in water which, however, do not exist in the presence of NPs. In the latter case, each PMAcOD molecule attaches mainly to the surface of a single NP, and SAXS unambiguously demonstrates that 99.9% volume fraction of NPs coated by PMAcOD are individual nanoparticles. The presence of extra oleic acid on the surface of NPs does not prevent encapsulation with PMAcOD due to PMAcOD cooperative interactions and an entropy increase. Fluorescence measurements of the pyrene uptake by NPs coated with PMAcOD demonstrate that pyrene can be absorbed by the hydrophobic double layer without disintegration of the double layer, revealing a high degree of stability of the PMAcOD coating.

Acknowledgment. This work has been supported, in part, by the NATO Science for Peace Program (Grant SfP-981438), NSF award 0631982, NIH award GM081029-01, NSF award 0220560, the IU FRSP grant, and the European Union FP6 Infrastructures Program (Design Study SAXIER, RIDS 011934). B.D. acknowledges support in part from the Indiana METACyt Initiative of Indiana University, funded in part through a major grant from the Lilly Endowment, Inc. The measurements at the EMBL beamline X33 at DESY were made within the projects SAXS-06-29 and SAXS-07-29. The authors thank Prof. Francoise Winnik (University of Montreal) for helpful discussions of pyrene experiments.

Supporting Information Available: TEM, XRD, magnetic measurement data, FTIR, and SAXS. This material is available free of charge via the Internet at http://pubs.acs.org.

References and Notes

(1) Sun, S.; Zeng, H. *J. Am. Chem. Soc.* **2002**, *124* (28), 8204.
(2) Frolov, G. I. *Tech. Phys.* **2001**, *46* (12), 1537.
(3) Lu, A.-H.; Salabas, E. L.; Schueth, F. *Angew. Chim. Int. Ed.* **2007**, *46* (8), 1222, and references therein.
(4) Sestier, C.; Da-Silva, M. F.; Sabolovic, D.; Roger, J.; Pons, J. N. *Electrophoresis* **1998**, *19* (7), 1220.
(5) Racuciu, M.; Creanga, D. E.; Calugaru, G. *J. Optoelectron. Adv. Mater.* **2005**, *7* (6), 2859.
(6) Bonini, M.; Wiedenmann, A.; Baglioni, P. *J. Appl. Crystallogr.* **2007**, *40* (S1), s254.
(7) Chang, S. Y.; Zheng, N.-Y.; Chen, C.-S.; Chen, C.-D.; Chen, Y.-Y.; Wang, C. R. C. *J. Am. Soc. Mass Spectrom.* **2007**, *18* (5), 910.
(8) Bulte, J. W.; Kraitchman, D. L. *NMR Biomed.* **2004**, *17*, 484.
(9) Mulder, W. J. M.; Strijkers, G. J.; van Tilborg, G. A. F.; Griffioen, A. W.; Nicolay, K. *NMR Biomed.* **2006**, *19* (1), 142.
(10) Medarova, Z.; Pham, W.; Farrar, C.; Petkova, V.; Moore, A. *Nat. Med.* **2006**, *13* (3), 372.
(11) Kumagai, M.; Imai, Y.; Nakamura, T.; Yamasaki, Y.; Sekino, M.; Ueno, S.; Hanaoka, K.; Kikuchi, K.; Nagano, T.; Kaneko, E.; Shimokado, K.; Kataoka, K. *Colloids Surf. B* **2007**, *56* (1−2), 174.
(12) Chemla, Y. R.; Grossman, H. L.; Poon, Y.; McDermott, R.; Stevens, R.; Alper, M. D.; Clarke, J. *Proc. Nat. Acad. Sci.* **2000**, *97* (26), 14268.
(13) Ivkov, R.; DeNardo, S. J.; Miers, L. A.; Natarajan, A.; Foreman, A. R.; Gruettner, C.; Adamson, G. N.; DeNardo, G. L. In *Development of tumor targeting magnetic nanoparticles for cancer therapy*, NSTI Nanotech 2006, Boston, MA, 2006; Nano Science and Technology Institute: Boston, MA, 2006; pp 21.
(14) Talapin, D. V.; Shevchenko, E. V.; Weller, H. Synthesis and Characterization of Magnetic Nanoparticles. In *Nanoparticles*; Schmid, G., Ed.; Wiley-VCH: Weinheim, 2004; p 199.
(15) Park, T.-J.; Papaefthymiou, G. C.; Viescas, A. J.; Moodenbaugh, A. R.; Wong, S. S. *Nano Lett.* **2007**, *7* (3), 766.
(16) Rong, C.-B.; Li, D.; Nandwana, V.; Poudyal, N.; Ding, Y.; Wang, Z. L.; Zeng, H.; Liu, J. P. *Adv. Mater.* **2006**, *18* (22), 2984.
(17) Li, Z.; Chen, H.; Bao, H.; Gao, M. *Chem. Mater.* **2004**, *16* (8), 1391.
(18) Redl, F. X.; Black, C. T.; Papaefthymiou, G. C.; Sandstrom, R. L.; Yin, M.; Zeng, H.; Murray, C. B.; O'Brien, S. P. *J. Am. Chem. Soc.* **2004**, *126* (44), 14583.
(19) Yu, W. W.; Falkner, J. C.; Yavuz, C. T.; Colvin, V. L. *Chem. Comm.* **2004**, (20), 2306.
(20) Park, J.; An, K.; Hwang, Y.; Park, J.-G.; Noh, H.-J.; Kim, J.-Y.; Park, J.-H.; Hwang, N.-M.; Hyeon, T. *Nat. Mater.* **2004**, *3* (12), 891.
(21) Kwon, S. G.; Piao, Y.; Park, J.; Angappane, S.; Jo, Y.; Hwang, N.-M.; Park, J.-G.; Hyeon, T. *J. Am. Chem. Soc.* **2007**, *129* (41), 12571.
(22) Jun, Y.-W.; Huh, Y.-M.; Choi, J.-S.; Lee, J.-H.; Song, H.-T.; Kim, S.; Yoon, S.; Kim, K.-S.; Shin, J.-S.; Suh, J.-S.; Cheon, J. *J. Am. Chem. Soc.* **2005**, *127* (16), 5732.
(23) Gussin, H. A.; Tomlinson, I. D.; Little, D. M.; Warnement, M. R.; Qian, H.; Rosenthal, S. J.; Pepperberg, D. R. *J. Am. Chem. Soc.* **2006**, *128* (49), 15701.
(24) Zhang, Q.; Gupta, S.; Emrick, T.; Russell, T. P. *J. Am. Chem. Soc.* **2006**, *128* (12), 3898.
(25) Han, G.; Ghosh, P.; Rotello, V. M. *Nanomedicine* **2007**, *2* (1), 113.
(26) Hostetler, M. J.; Templeton, A. C.; Murray, R. W. *Langmuir* **1999**, *15* (11), 3782.
(27) Wan, S.; Huang, J.; Guo, M.; Zhang, H.; Cao, Y.; Yan, H.; Liu, K. *J. Biomed. Mater. Res.* **2007**, *80A* (4), 946.
(28) Kang, Y.; Taton, T. A. *Macromolecules* **2005**, *38* (14), 6115.
(29) Korth, B. D.; Keng, P.; Shim, I.; Bowles, S. E.; Tang, C.; Kowalewski, T.; Nebesny, K. W.; Pyun, J. *J. Am. Chem. Soc.* **2006**, *128* (20), 6562.
(30) Nitin, N.; LaConte, L. E. W.; Zurkiya, O.; Hu, X.; Bao, G. *J. Biol. Inorg. Chem.* **2004**, *9* (6), 706.
(31) Dubertret, B.; Skourides, P.; Norris, D. J.; Noireaux, V.; Brivanlou, A. H.; Libchaber, A. *Science* **2002**, *298* (5599), 1759.
(32) Lim, Y. T.; Lee, K. Y.; Lee, K.; Chung, B. H. *Biochem. Biophys. Res. Commun.* **2006**, *344* (3), 926.
(33) Huang, X.; Bronstein, L. M.; Retrum, J. R.; Dufort, C.; Tsvetkova, I.; Aniagyei, S.; Stein, B.; Stucky, G.; McKenna, B.; Remmes, N.; Baxter, B.; Kao, C. C.; Dragnea, B. *Nano Lett.* **2007**, *7* (8), 2407.
(34) Shtykova, E. V.; Huang, X.; Remmes, N.; Baxter, D.; Stein, B. D.; Dragnea, B.; Svergun, D. I.; Bronstein, L. M. *J. Phys. Chem. C* **2007**, *111* (49), 18078.
(35) Pellegrino, T.; Manna, L.; Kudera, S.; Liedl, T.; Koktysh, D.; Rogach, A. L.; Keller, S.; Raedler, J.; Natile, G.; Parak, W. J. *Nano Lett.* **2004**, *4* (4), 703.
(36) Yu, W. W.; Chang, E.; Sayes, C. M.; Drezek, R.; Colvin, V. L. *Nanotechnology* **2006**, *17* (17), 4483.
(37) Di Corato, R.; Quarta, A.; Piacenza, P.; Ragusa, A.; Figuerola, A.; Buonsanti, R.; Cingolani, R.; Manna, L.; Pellegrino, T. *J. Mater. Chem.* **2008**, *18* (17), 1991.
(38) Feigin, L. A.; Svergun, D. I. *Structure Analysis by Small-Angle X-ray and Neutron Scattering*; Plenum Press: New York, 1987.
(39) Svergun, D. I.; Shtykova, E. V.; Kozin, M. B.; Volkov, V. V.; Dembo, A. T.; Shtykova, E. V. J.; Bronstein, L. M.; Platonova, O. A.; Yakunin, A. N.; Valetsky, P. M.; Khokhlov, A. R. *J. Phys. Chem. B.* **2000**, *104*, 5242.
(40) Svergun, D. I.; Kozin, M. B.; Konarev, P. V.; Shtykova, E. V.; Volkov, V. V.; Chernyshov, D. M.; Valetsky, P. M.; Bronstein, L. M. *Chem. Mater.* **2000**, *12*, 3552.
(41) Bronstein, L. M.; Sidorov, S. N.; Zhirov, V.; Zhirov, D.; Kabachii, Y. A.; Kochev, S. Y.; Valetsky, P. M.; Stein, B.; Kiseleva, O. I.; Polyakov, S. N.; Shtykova, E. V.; Nikulina, E. V.; Svergun, D. I.; Khokhlov, A. R. *J. Phys. Chem. B* **2005**, *109*, 18786.
(42) Shtykova, E. V.; Svergun, D. I.; Chernyshov, D. M.; Khotina, I. A.; Valetsky, P. M.; Spontak, R. J.; Bronstein, L. M. *J. Phys. Chem. B* **2004**, *108*, 6175.
(43) Bronstein, L. M.; Linton, C.; Karlinsey, R.; Ashcraft, E.; Stein, B.; Svergun, D. I.; Kozin, M.; Khotina, I. A.; Spontak, R. J.; Werner-Zwanziger, U.; Zwanziger, J. W. *Langmuir* **2003**, *19*, 7071.
(44) Bronstein, L. M.; Dixit, S.; Tomaszewski, J.; Stein, B.; Svergun, D. I.; Konarev, P. V.; Shtykova, E.; Werner-Zwanziger, U.; Dragnea, B. *Chem. Mater.* **2006**, *18* (9), 2418.
(45) Svergun, D. I.; Shtykova, E. V.; Dembo, A. T.; Bronstein, L. M.; Platonova, O. A.; Yakunin, A. N.; Valetsky, P. M.; Khokhlov, A. R. *J. Chem. Phys.* **1998**, *109*, 11109.
(46) Bronstein, L. M.; Platonova, O. A.; Yakunin, A. N.; Yanovskaya, I. M.; Valetsky, P. M.; Dembo, A. T.; Makhaeva, E. E.; Mironov, A. V.; Khokhlov, A. R. *Langmuir* **1998**, *14*, 252.
(47) Svergun, D. I. *Biophys. J.* **1999**, *76*, 2879.
(48) Svergun, D. I.; Barberato, C.; Koch, M. H. J. *J. Appl. Crystallogr.* **1995**, *28*, 768.

(49) Petoukhov, M. V.; Svergun, D. I. *Biophys. J.* **2005**, *89*, 1237.
(50) Shtykova, E. V.; Shtykova, E. V., Jr.; Volkov, V. V.; Konarev, P. V.; Dembo, A. T.; Makhaeva, E. E.; Ronova, I. A.; Khokhlov, A. R.; Reynaers, H.; Svergun, D. I. *J. Appl. Crystallogr.* **2003**, *36*, 669.
(51) Volkov, V. V.; Lapuk, V. A.; Kayushina, R. L.; Shtykova, E. V.; Varlamova, E. Y.; Malfois, M.; Svergun, D. I. *J. Appl. Crystallogr.* **2003**, *36*, 503.
(52) Bronstein, L. M.; Huang, X.; Retrum, J.; Schmucker, A.; Pink, M.; Stein, B. D.; Dragnea, B. *Chem. Mater.* **2007**, *19* (15), 3624.
(53) Bronstein, L. M.; Huang, X.; Retrum, J. R.; Schmucker, A. L.; Pink, M.; Stein, B. D.; Dragnea, B. *Chem. Mater.* **2007**, *19*, 3624.
(54) Roessle, M. W.; Klaering, R.; Ristau, U.; Robrahn, B.; Jahn, D.; Gehrmann, T.; Konarev, P.; Round, A.; Fiedler, S.; Hermes, C.; Svergun, D. *J. Appl. Crystallogr.* **2007**, *40*, s190.
(55) Konarev, P. V.; Volkov, V. V.; Sokolova, A. V.; Koch, M. H. J.; Svergun, D. I. *J. Appl. Crystallogr.* **2003**, *36*, 1277.
(56) Svergun, D. I. *J. Appl. Crystallogr.* **1992**, *25*, 495.
(57) MSI Cerius2, Version 3.5.; Molecular Simulation Inc.: San Diego, CA, 1997.
(58) Malardier-Jugroot, C.; Van de Ven, T. G. M.; Cosgrove, T.; Richardson, R. M.; Whitehead, M. A. *Langmuir* **2005**, *21* (22), 10179.
(59) Whiles, J. A.; Deems, R.; Vold, R. R.; Dennis, E. A. *Bioorg. Chem.* **2002**, *30* (6), 431.
(60) Dubois, M.; Lizunov, V.; Meister, A.; Gulik-Krzywicki, T.; Verbavatz, J. M.; Perez, E.; Zimmerberg, J.; Zemb, T. *Proc. Nat. Acad. Sci.* **2004**, *101* (42), 15082.
(61) Gutberlet, T.; Hoell, A.; Kammel, M.; Frank, J.; Katsaras, J. *Appl. Phys. A: Mater. Sci. Process.* **2002**, *74* (2), S1260.
(62) Luchette, P. A.; Vetman, T. N.; Prosser, R. S.; Hancock, R. E. W.; Nieh, M.-P.; Glinka, C. J.; Krueger, S.; Katsaras, J. *Biochim. Biophys. Acta* **2001**, *1513* (2), 83.
(63) Kalyanasundaram, K.; Thomas, J. K. *J. Am. Chem. Soc.* **1977**, *99*, 72039–72044.
(64) Winnik, F. M.; Davidson, A. R.; Hamer, G. K.; Kitano, H. *Macromolecules* **1992**, *25* (7), 1876.
(65) Winnik, F. M.; Regismond, S. T. A. *Colloids Surf., A* **1996**, *118* (1/2), 1.
(66) Baker, L. A.; Crooks, R. M. *Macromolecules* **2000**, *33* (24), 9034.
(67) Turro, N. J.; Lakshminarasimhan, P. H.; Jockusch, S.; O'Brien, S. P.; Grancharov, S. G.; Redl, F. X. *Nano Lett.* **2002**, *2* (4), 325.

JP8053636